JOURNAL OF MATERIALS SCIENCE 5 (1970) 445–452

Field-ion Microscopy of Uranium Dioxide

R. MORGAN*
Central Electricity Generating Board, Berkeley Nuclear Laboratories, Berkeley, Gloucs, UK

Specimens of uranium dioxide have been prepared for field-ion microscopy by diamond-sawing followed by chemical polishing and electro-polishing. Hydrogen-ion and argon-ion microscopy have been found satisfactory. Hydrogen images are slightly unstable, owing to field-induced corrosion, but argon images are completely stable at the best-image field. Argon-ion images are improved by raising the temperature of the specimen coolant from 78 to 113° K; this also causes a large reduction in the best-image voltage, owing to an improvement in the electrical conductivity of the specimen. The imaging element in hydrogen-ion micrographs is uranium.

1. Introduction

The field-ion microscope [1] is a useful tool for studying solids at very high resolution. An introduction to the technique has been published by Ralph and Southon [2], and the review articles by Müller [3] and Brandon [4] provide a survey of its applications. The book by Hren and Ranganathan [5] is a useful and up-to-date account of the theory of field-ion microscopy and of the interpretation of field-ion micrographs.

The most valuable advantage of the field-ion microscope is its ability to resolve the structure of a specimen on an atomic scale. The most obvious potential applications to uranium dioxide are the study of surface diffusion and the structure of fission-fragment tracks.

Most of the materials studied up to now have been refractory metals and their dilute alloys. Compounds have proved very difficult to study, for reasons which in most cases are uncertain. Meakin [6] and Meakin and Raghavan [7] have obtained images from tantalum carbide and tungsten carbide, and subsequently (Meakin [8]) from various other refractory materials. French and Richman [9] have obtained images from tungsten carbides prepared by carbonising tungsten. Smith *et al* [10] have had limited success in imaging titanium carbide. Ralph and the present author [11] have obtained images from cementite (Fe_3C) in the form of precipitates in steel, and Schwartz *et al* [12] have obtained images from alloy carbides in steel. Studies of oxides have generally been confined to the early stages of oxidation (see, for example, Ehrlich [13], Cranstoun [14], Cranstoun and Anderson [15]) except for the work of Fortes and Ralph [16] on iridium oxidation and Brenner and McVeagh [17] on tungsten oxidation.

In the present work an attempt has been made to study specimens prepared from bulk oxide, rather than from oxidised metal specimens.

2. Special Preparation

A pellet of sintered polycrystalline natural uranium dioxide of composition $UO_{<2.002}$ and density $> 96\%$ theoretical, was sawn into bars of 1 mm square cross-section using a diamond wheel.

Various methods of polishing were tried [18]. Electro-polishing was found to be too slow, and chemical polishing, although rapid, gave a very poor surface finish and often produced chisel-shaped specimens having very different tip radii in different profiles. A two-stage procedure was finally adopted, in which chemical polishing was used to develop the necessary waisted profile, and electro-polishing was used to finish.

The chemical polishing was done as follows. The lower end (about 2 mm) of the bar was masked off with Araldite, and the bar was lowered to a depth of about 6 mm into a solution consisting of 20 ml 90% orthophosphoric acid, 10 ml glacial acetic acid and 2 ml concentrated

*Now at the School of Physical Sciences, The New University of Ulster, Coleraine, Co Londonderry, Northern Ireland.

nitric acid, at a temperature of 120° C (Manley [19]). A waist developed just above the Araldite layer (fig. 1). It was found necessary to move the specimen continuously during polishing to prevent pitting at the meniscus. Polishing was continued until the waist was reduced to about 0.05 mm.

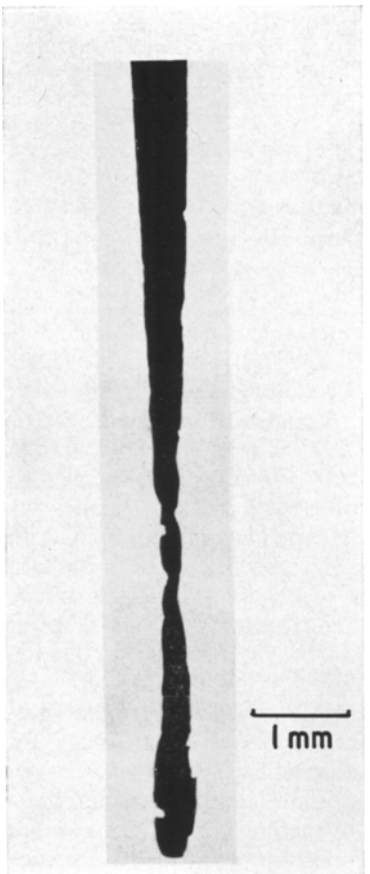

Figure 1 Profile of a typical UO_2 specimen after chemical polishing (optical micrograph).

The electro-polishing was done in a solution of 310 ml 90% orthophosphoric acid, 38 g chromium trioxide, 67 ml concentrated sulphuric acid, and 120 ml water, used at room temperature with a stainless steel cathode. (R. M. Cornell, private communication.) Because of the low electrical conductivity of uranium dioxide (between 10^{-4} and 10^{-6} ohm^{-1} at 25° C) it was found necessary to use a high voltage ($\simeq$ 60 V), and even so the polishing current was only about 200 μA. Most of the attack occurred at the meniscus, and in order to minimise the duration of the polishing, the thinnest part of the specimen was placed just beneath the meniscus.

A profile of a typical specimen is shown in figs. 2a and b.

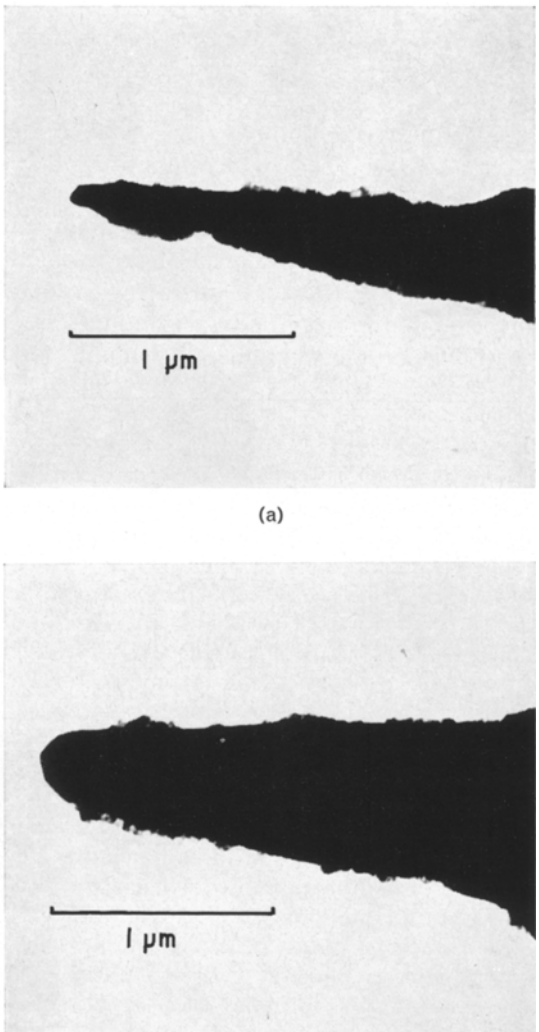

Figure 2 Profiles of a typical specimen after electro-polishing showing maximum and minimum radii (electron micrographs).

3. Specimen Mounting

Uranium dioxide cannot be spot-welded without risking fracture. In earlier work using a lightly-baked vacuum system, the specimen was glued with silver-loaded Araldite into a nickel tube which was then pushed over the pin of the specimen-holder. In later work using a baked

ultra-high-vacuum system, Araldite could not be used, and the specimen was held by crimping the nickel tube lightly on to the tapering shank.

4. Imaging

4.1. Hydrogen-ion Microscopy

Hydrogen-ion microscopy, with the specimen cooled by liquid nitrogen (78° K), has been found satisfactory for imaging uranium dioxide. As is usually the case with hydrogen, there is a continuous field-induced corrosion whose rate depends on the applied field, the hydrogen pressure and the pressure of contaminants, but the rate of corrosion is slow (several seconds per {111} plane removed). A hydrogen-ion image of uranium dioxide is shown in fig. 3.

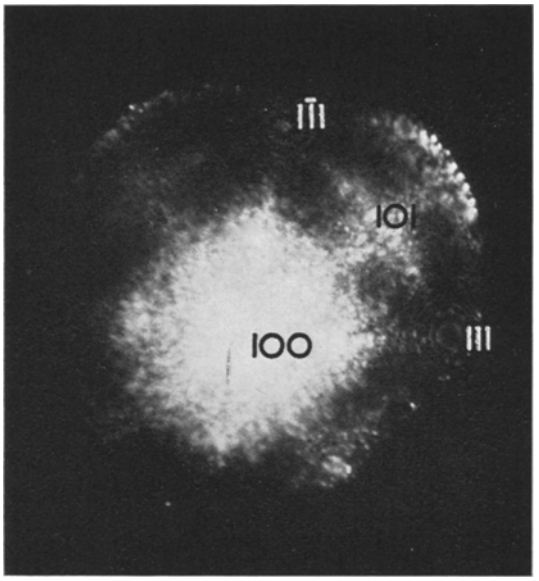

Figure 3 Hydrogen-ion micrograph of uranium dioxide. 16 kV, 1.5×10^{-3} torr H_2, 78° K.

4.2. Argon-ion Microscopy

Although hydrogen-ion images are satisfactory for many purposes, the continuous corrosion is a nuisance, and attempts were therefore made to image uranium dioxide with inert gases. It was not possible to obtain a stable image with helium or neon at 78° K, and no improvement was apparent on lowering the temperature of the specimen coolant by pumping. Argon-ion microscopy, with an image converter, appeared to be promising, but in a conventional oil-pumped microscope with a background pressure of about 5×10^{-8} torr the surface of the specimen was obscured by contamination, and little detail could be seen.

An ultra-high vacuum microscope was constructed to the author's design [20] by Vacuum Generators Limited. A bakeable magnetically focused mesh type image converter was constructed by Mr S. Evans and the author to a design by Turner [21]. A vacuum of better than 2×10^{-10} torr was obtained without difficulty, and this was found to be quite satisfactory for argon-ion microscopy.

An argon-ion micrograph of uranium dioxide, taken with a specimen coolant temperature of 78° K, is shown in fig. 4. The resolution is little better than that obtained with hydrogen (fig. 3) and the subjective impression of quality is rather worse, but the image was completely stable at the best-image field. Field-evaporation started at about 110% of the best-image voltage, and could be done without risk of specimen failure. Hydrogen-etching (Müller *et al* [22]) was also possible.

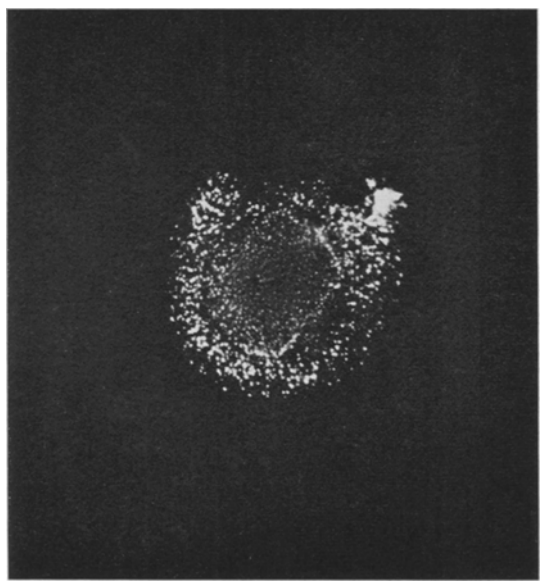

Figure 4 Argon-ion micrograph of uranium dioxide. 46.5 kV, 1×10^{-3} torr Ar, 78° K. The small size of the image is evident by comparison with the other micrographs, all of which are printed at the same photographic magnification.

When the specimen coolant temperature was raised to 113° K (melting iso-pentane) the image was considerably improved (figs. 5 and 6). There was also a drastic change in best-image voltage; in a typical case the best-image voltage at 70° K

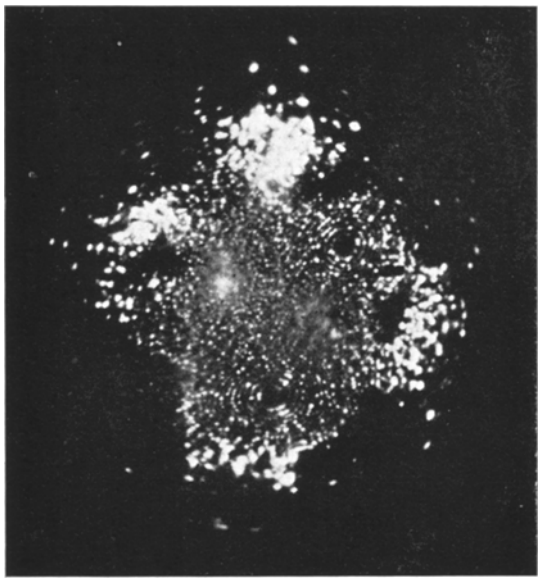

Figure 5 Argon-ion micrograph of uranium dioxide. 8.4 kV, 1×10^{-3} torr Ar, 113° K.

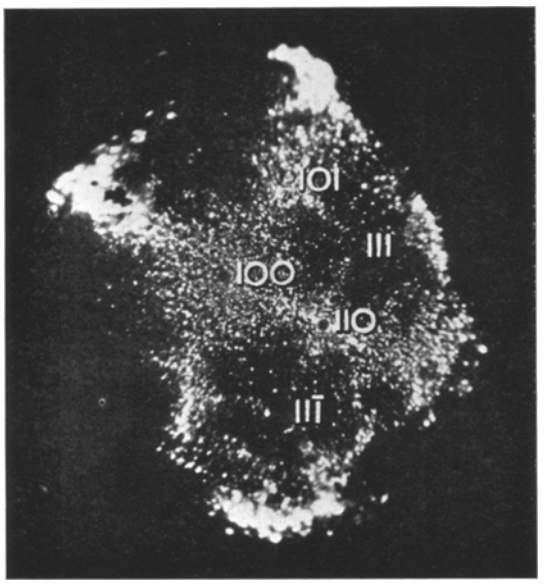

Figure 6 The same specimen as in fig. 5 after further field-evaporation. 13.1 kV, 1×10^{-3} torr Ar, 113° K.

was 40 kV, and at 113° K was 11 kV. In addition, the diameter of the image on the screen increased by at least 20% on raising the temperature from 78 to 113° K.

4.3. Explanation of the Effects of Temperature Change

The degradation of the image at low temperature has been observed for other image gases (Müller, [23] made the earliest report of this effect), and it has been explained by Müller [24] as being due to the thermally accommodated gas atoms staying within the zone of forbidden ionisation, thus failing to contribute to the image.

The change in best-image voltage with temperature is probably due to a change in mobility of the current-carrying species. Nagels, Devreese and Denayer [25] and Devreese, De Conninck and Pollak [26], have studied the temperature-dependence of conductivity of uranium dioxide, and they found an exponential change of conductivity with temperature. For uranium dioxide of the same degree of non-stoichiometry as the present author's specimens, they find that at 90° K, the conductivity is of the order of 10^{-9} ohm^{-1} cm^{-1}, rising to a value of the order of 10^{-8} ohm^{-1} cm^{-1} at 100° K. Because the ion current in the microscope, and the shape and dimensions of the specimen, have not been measured, it is not possible to estimate the voltage drop in the vicinity of the tip, but the observed temperature-dependence of the best-image voltage implies that the voltage drop at 78° K may be several times greater than the expected best-image voltage for a good conductor.

The change of image size on changing the specimen temperature can be explained qualitatively in the following manner. At 78° K the bulk of the specimen is at a higher positive voltage than the tip, and there is therefore a relatively large region of higher positive potential behind the field-ionising region. This can be expected to behave to some extent like a charged plane, and thus to bend the ion beams from their approximately radial paths into paths more nearly perpendicular to this notional plane, i.e. to bend them inwards, so causing the observed image contraction. When the specimen temperature is raised, the conductivity increases; the bulk of the specimen is no longer at a very different potential from that of the tip, and the image therefore enlarges, back to its usual size.

If the foregoing explanation of the change of image size is correct, the image of a poorly-conducting specimen should enlarge when the specimen voltage is lowered below the threshold field, because the ion current falls off very sharply below the threshold, and the potential drop along the specimen should be much reduced. This change of image size with voltage should be more noticeable when the specimen

has a higher resistivity, i.e. the effect should be greater at 78° K than at 113° K. This effect has indeed been observed, and it is much more pronounced at 78° K than at 113° K.

There is therefore strong evidence to suggest that the changes of best-image voltage and image diameter with coolant temperature are due to the high resistivity and the high negative temperature coefficient of resistance of uranium dioxide at low temperatures.

5. Identification of the Visible Element

5.1. Introduction

This section considers the question of whether the atoms which are visible are uranium, or oxygen, or both. Following Southworth [27], and Southworth and Ralph [28], one might expect one of the following circumstances to exist:

(i) Neither species is evaporated preferentially, and therefore both U and O atoms are retained in the field-evaporated end form. U, being more positively charged than O, has a higher probability of causing ionisation of the image gas, and should therefore be brighter than O. In the extreme, this leads to invisibility of oxygen.

(ii) One species is preferentially evaporated from the field-evaporated end form and does not appear in the image. Since U is more positively charged than O, the U atoms should evaporate more easily. In the extreme, this leads to non-appearance of uranium.

(iii) Of the different mechanisms and results of (i) and (ii), one mechanism might predominate in some regions of the micrograph, and the other mechanism in other regions.

Two methods have been used to obtain an answer to this question and these will now be discussed.

5.2. Method of Relative Prominences of Poles

5.2.1. Theory

The "prominence" of a pole in a field-ion image is basically a qualitative judgement, but it can be made more quantitative by equating the prominence of a pole (*hkl*) with the maximum diameter on the micrograph of the innermost ring of atoms surrounding the pole (*hkl*), i.e. the maximum diameter of the topmost layer of atoms in the plane (*hkl*).

Wald [29] has shown that in a pure metal the prominence of a pole (*hkl*) is approximately proportional to the reticular density of atoms in the plane (*hkl*). An alternative approach was made by Drechsler and Liepack [30], who suggested that the prominences of poles are determined by their inter-layer spacing. This suggestion was developed by Moore and Ranganathan [31] using computer simulation, and they found very satisfactory correlation between inter-layer spacing and prominence.

In a pure metal the reticular density of a plane must be proportional to the inter-layer spacing of that plane, and so the two approaches are equivalent. This is not necessarily true in more complicated structures, and it is open to discussion whether reticular densities or inter-layer spacings should be used in such circumstances. Following a discussion with H. N. Southworth (private communication), the present author regards inter-layer spacing as the more useful criterion, since it is easily shown that the maximum diameter L_{max} of the topmost layer of atoms (which was the definition of "prominence" given at the start of this section) is given approximately by

$$L_{max} \simeq (8dR)^{\frac{1}{2}} \text{ when } d \ll R\,,$$

where L_{max} = maximum diameter of the topmost layer of atoms on the plane (*hkl*); d = inter-layer spacing of (*hkl*); R = radius of tip. (Moore and Ranganathan, [31].) Consequently the prominence is proportional to L_{max} which is proportional to $d^{\frac{1}{2}}$.

5.2.2. Calculations of d for UO_2

Uranium dioxide has the CaF_2 structure (cf. standard texts on crystallography) with cell edge = 5.46 Å. The U atoms occupy a face-centred-cubic sub-lattice with cell edge = 5.46 Å, and the O atoms occupy a primitive cubic sub-lattice with cell edge = 2.73 Å. Consequently, if the uranium atoms are imaged, the order of prominence of the poles will be that of a face-centred-cubic structure, while if the oxygen atoms are imaged, the order of prominence will be that of a primitive cubic structure.

The inter-layer spacing d_{hkl} of planes (*hkl*) in the oxygen sub-lattice were calculated from

$$d_{hkl} = a(h^2 + k^2 + l^2)^{-\frac{1}{2}}$$

(where a = oxygen cell edge = 2.73 Å) and are tabulated in table I.

The inter-layer spacings of planes in the uranium sub-lattice were calculated in the same way, observing the usual doubling rules for fcc and these are tabulated in table II.

The possibility exists of both species contribu-

TABLE I Inter-layer spacings in oxygen sub-lattice

Plane *hkl*	Inter-layer spacings Å	
100	2.73	
110	1.93	
111	1.58	Order of prominence
210	1.22	expected if oxygen
211	1.11	images
221	0.91	
310	0.86	{100}, {110}, {111}
311	0.82	
320	0.76	
321	0.73	

TABLE II Inter-layer spacings in uranium sub-lattice.

Plane *hkl*	Inter-layer spacing Å	
111	3.15	
200	2.73	
220	1.93	Order of prominence
311	1.65	expected if uranium
331	1.25	images
420	1.22	
422	1.11	{111}, {100}, {110}
511	1.05	
531	0.92	
442	0.91	

TABLE III Inter-layer spacings considering both species

Plane *hkl*	Inter-layer spacing Å	
110	1.93	
111	1.58 or 0.79	Order of prominence
100	1.37	expected if both species
211	1.11	image
310	0.86	{110}, {111}, {100}, {211}
311	0.82 or 0.41	alternating with
321	0.73	{110}, {100}, {211}, {310}
210	0.61	
221	0.45	
320	0.38	

ting almost equally to the image. Inter-layer spacings were therefore calculated for this state of affairs, with the aid of a Mathatron computer [32], and the results are tabulated in table III.

5.2.3. Results

Indexed micrographs of uranium dioxide are shown in figs. 3 and 6; the indexing has been done by symmetry. It is evident that {111} is the most prominent in all cases, indicating that only the uranium atoms image. In the hydrogen-ion micrograph (fig. 3) the next pole in order of prominence is {100} followed by {110}, again indicating that only the uranium atoms are visible. In the argon-ion micrographs, measurements of L_{max} indicate that {100} is more prominent than {110}, which indicates again that only the uranium atoms are imaging.

It can be concluded, therefore, that in both hydrogen-ion and argon-ion micrographs of uranium dioxide, only the uranium atoms are visible, at least near the prominent poles.

5.3. Method of Inter-layer Spacing

5.3.1. Theory

Drechsler and Wolf [33] have shown that the spacing between layers of atoms on a pole $(h_1k_1l_1)$ can be determined from

$$d = \frac{R}{n}(1 - \cos\alpha)$$

where d = spacing between layers, R = radius of curvature of the specimen in the region of interest, α = angle between the pole $(h_1k_1l_1)$ and a neighbouring pole $(h_2k_2l_2)$, and n = number of rings in the image between the poles $(h_1k_1l_1)$ and $(h_2k_2l_2)$.

n can be measured from the micrograph, α can be determined either from the known crystal structure or by measurement on a stereogram, and R can be measured as described below. Hence d can be calculated.

In most planes in the uranium dioxide structure, the spacing between one uranium layer and the next is different from the spacing between one oxygen layer and the next. If the inter-layer spacing for a particular pole is measured from the micrographs, and compared with the spacings expected at that pole, it is possible to determine which element is imaging.

This procedure has been used by Southworth and Ralph [34] in a study of Pt–Co alloy. In their work the radius of curvature of the specimen was determined from the voltage applied to the specimen at the best-image field. In the present work this method was not applicable because of the large voltage drop along the specimen (section 4). It was therefore necessary to measure the radius by another method.

5.3.2. Radius Measurement

If an electron micrograph is taken of the specimen in profile, a measurement of the radius can

be made. Field-ion specimens of uranium dioxide are often elliptical in cross-section, and it is therefore necessary to measure the radius of curvature in a series of profiles during which the specimen is rotated 180° about its axis. A special specimen holder was constructed to make this possible [32].

Having obtained electron micrographs of a specimen in a series of profiles, with each profile identified by means of a diffraction pattern, the radius of the tip was measured by fitting a circle to the profile in each micrograph. So as to eliminate any subjective effects, a numerical procedure was devised. A micro-densitometer was used to scan the micrograph and hence to define the position of the edge in terms of the values of two rectangular co-ordinates. A circle was fitted to these values by a statistical method, using a Mathatron computer [32].

Finally the radius of the circle was divided by the corrected magnification of the electron microscope, and the resulting value of the tip radius was inserted into the equation of section 5.3.1. In each case, that electron micrograph profile was used which corresponded to the zone along which ring-counting was done; in this way errors due to ellipticity of cross-section were prevented.

5.3.3. Results

Argon-ion microscopy of uranium dioxide has only recently become possible, and no measurements have been made on argon-ion micrographs.

Eight separate measurements have been made near {1 1 1} poles in hydrogen-ion micrographs, and the results are summarised in table IV. The average value of d is found to be $d = 2.97 \pm 1.67$ Å. The spacing between layers of uranium at the {1 1 1} pole is 3.17 Å, while that between layers of oxygen is 1.59 Å. Although the large error prohibits an unambiguous conclusion from these results, it is likely that the imaging species is uranium rather than oxygen. This conclusion becomes more likely when the effect of systematic error (section 5.3.4) is taken into consideration, because the value obtained for d is expected to err on the low side of the correct value. It is therefore fairly safe to conclude that in the vicinity of the {1 1 1} poles, only the uranium atoms are visible.

TABLE IV Results of ring-counts

No. of rings n	Angle α, °	Radius R, Å	Spacing d, Å
5	10.7	700	2.45
5	8.5	950	2.09
10	27.4	580	5.90
7	21.3	580	5.66
5	6.0	1160	1.28
5	8.0	808	1.57
6	11.0	744	2.28
6	11.5	744	2.49
			2.965 ± 1.67 Å

This agrees with the result obtained in section 5.2.

5.3.4. Errors

The large scatter in the results arises because in micrographs of uranium dioxide it is not possible to count rings between two poles, since discernible rings exist only near to prominent poles. The counting is therefore done along a prominent zone, from the centre of the ring system to the point where rings cease to be discernible, and the angle between this point and the pole is measured by interpolation using a Wulff net. It is difficult to measure on a net of 300 mm diameter to an accuracy of better than ½°, and for a typical set of figures an error of this magnitude generates an error in the calculated ring spacing of about 10%. In most cases the accuracy is rather worse than ± ½° because of inaccuracies of measurement in transferring the information from the micrograph to the net, so the resulting accuracy of the ring-spacing is rather poor.

A systematic error occurs because all the ring-counts are made in the vicinity of the prominent pole, where the profile is somewhat flattened, i.e. the radius is greater than the average over the whole tip. The radius meaured from the electron micrographs is an average value, and it is therefore smaller than that which is strictly appropriate to the region being used for ring-counts. A low value of the radius leads to a low value for d in the equation of Drechsler and Wolf (section 5.3.1), and consequently the measured values of layer spacings are low. For the case of tungsten, where the flattening of the {1 1 0} poles is typically 10 Å on a tip of 360 Å mean radius [33], the radius varies by a factor of 2 over the specimen. The flattening of the poles in uranium dioxide is very much less (it is too small to be measured by electron microscopy) but it is probably still sufficient to cause some systematic error in the layer spacings.

6. Conclusions

(i) Specimens of uranium dioxide can be prepared for field-ion microscopy by diamond-sawing the material into square-section bars, followed by chemical polishing into a waisted shape, and finally electro-polishing until the lower end falls off.

(ii) Satisfactory field-ion images of uranium dioxide can be obtained by hydrogen-ion and by argon-ion microscopy. Hydrogen-ion images are slightly unstable, owing to field-induced corrosion of the specimen. Argon images are completely stable at the best-image voltage. Field-evaporation can be done without risk of specimen failure.

(iii) Argon-ion images are improved by raising the temperature of the specimen coolant from 78° K (liquid nitrogen) to 113° K (melting isopentane). This also causes a large reduction in the best-image voltage, owing to an improvement in the electrical conductivity of the specimen.

(iv) In hydrogen-ion micrographs, only the uranium atoms are visible, at least near the prominent poles. The same conclusion is probably true for argon-ion micrographs, but it would be desirable to have quantitative results before making a definite statement.

Acknowledgement

The author acknowledges the assistance of Dr P. J. Turner of Cambridge University in the design of the image converter, and of Mr S. Evans of this Laboratory in the construction of the converter. He thanks Dr H. N. Southworth of Birmingham University for discussions on image interpretation and for his comments on the manuscript. He thanks his colleagues, and especially Dr J. T. Buswell and Dr B. C. Masters, for their advice and comments. This paper is published by permission of the Central Electricity Generating Board.

References

1. E. W. MÜLLER, *Z. Physik* **131** (1951) 136.
2. B. RALPH and M. J. SOUTHON, *Sci. J.* **2** (1966) 51.
3. E. W. MÜLLER, *Adv. Electronics Electron Phys.* **13** (1960) 83.
4. D. G. BRANDON, *Brit. J.A.P.* **14** (1963) 474.
5. J. J. HREN and S. RANGANATHAN, "Field Ion Microscopy" (Plenum Press, New York, 1968).
6. J. D. MEAKIN, *Phil. Mag.* **17** (1968) 865.
7. J. D. MEAKIN and D. RAGHAVAN, 15th Field Emission Symposium, Bonn, 1968.
8. J. D. MEAKIN, 16th Field Emission Symposium, Pittsburgh, 1969.
9. R. D. FRENCH and M. H. RICHMAN, *Phil. Mag.* **18** (1968) 471.
10. D. A. SMITH, B. RALPH, and W. S. WILLIAMS, *ibid* **16** (1967) 415.
11. R. MORGAN and B. RALPH, *J. Iron Steel Inst.* **206** (1968) 1138.
12. D. M. SCHWARTZ, A. T. DAVENPORT, and B. RALPH, *Phil. Mag.* **18** (1968) 431.
13. G. EHRLICH, Proc. 3rd Int. Cong. on Catalysis, Amsterdam, 1964 (Published, 1965).
14. G. K. L. CRANSTOUN, 15th Field Emission Symposium, Bonn, 1968.
15. G. K. L. CRANSTOUN and J. S. ANDERSON, *Nature* **219** (1968) 365.
16. M. A. FORTES and B. RALPH, *Proc. Roy. Soc.* **A307** (1968) 431.
17. S. S. BRENNER and W. J. MCVEAGH, *J. Electrochem. Soc.* **115** (1968) 1247.
18. R. MORGAN, CEGB internal report RD/B/N1230 (1968).
19. A. J. MANLEY, *J. Nucl. Matls* **15** (1965) 143.
20. R. MORGAN, CEGB internal report RD/B/N1455 (1969).
21. P. J. TURNER, P. CARTWRIGHT, M. J. SOUTHON, A. VAN OOSTROM, and B. W. MANLEY, *J. Sci. Instr.* Ser. 2, **2** (1969) 731.
22. E. W. MÜLLER, S. NAKAMURA, O. NISHIKAWA, and S. B. MCLANE, *J. Appl. Phys.* **36** (1965) 2496.
23. E. W. MÜLLER, *ibid* **27** (1956) 474.
24. *Idem, ibid* **28** (1957) 1.
25. P. NAGELS, J. DEVREESE, and M. DENAYER, *ibid* **35** (1964) 1175.
26. J. DEVREESE, R. DE CONNINCK, and H. POLLAK, *Phys. Stat. Sol.* **17** (1966) 825.
27. H. N. SOUTHWORTH, *Scripta Met.* **2** (1968) 551.
28. H. N. SOUTHWORTH and B. RALPH, *J. Micros.* **90** (1969) 167.
29. M. S. WALD, Ph.D. Thesis, Cambridge University, 1963.
30. M. DRECHSLER and H. LIEPACK, Colloq. Inter. CRNS, Nancy (1965) p. 49.
31. A. J. W. MOORE and S. RANGANATHAN, *Phil. Mag.* **16** (1967) 723.
32. R. MORGAN, CEGB internal report RD/B/N1502 (1969).
33. M. DRECHSLER and P. WOLF, 4th Int. Conf. on Electron Microscopy, Berlin, 1958 (Springer-Verlag, Berlin, 1960) p. 835.
34. H. N, SOUTHWORTH and B. RALPH, *Phil. Mag.* **14** (1966) 383.

Received 18 November 1969 and accepted 3 February 1970.